Metallophysics and Advanced Technologies
Металофіз. новітні технол.
Metallofiz. Noveishie Tekhnol.
2019, vol. 41, No. 7, pp. 941–952
https://doi.org/10.15407/mfint.41.07.0941
Reprints available directly from the publisher

STRUCTURE AND PROPERTIES OF NANOSCALE AND MESOSCOPIC MATERIALS

PACS numbers: 61.05.cp, 68.37.Ps, 68.55.J-, 73.61.At, 78.66.Bz, 81.15.Cd

Effect of Sputtering Power on Optoelectronic Properties of Iron-Doped Indium Saving Indium-Tin Oxide Thin Films

M. Ohtsuka, R. Sergiienko*, S. Petrovska**, B. Ilkiv**, and T. Nakamura

Institute of Multidisciplinary Research for Advanced Materials,
Tohoku University,
2 Chome-1-1 Katahira, Aoba Ward, Sendai,
Miyagi 980-0812, Japan
**Physico-Technological Institute of Metals and Alloys, N.A.S. of Ukraine,*
34/1 Academician Vernadsky Blvd.,
UA-03142 Kyiv, Ukraine
***I. M. Frantsevich Institute for Problems in Materials Science, N.A.S. of Ukraine,*
3 Academician Krzhyzhanovsky Str.,
UA-03142 Kyiv, Ukraine

Iron-doped indium-tin oxide (ITO) thin films with reduced to 50% mass indium oxide content are deposited onto glass substrates preheated at 523 K by co-sputtering of ITO and Fe_2O_3 targets in mixed argon-oxygen atmosphere. The influence of different radio frequency (RF) plasma power for deposition of Fe_2O_3 target on the electrical, optical, structural, and morphological properties of the films is investigated by means of four point probe, Ultraviolet–Visible–Infrared (UV–Vis–IR) spectroscopy, X-ray diffraction and atomic force microscopy methods. The volume resistivity of 930 μΩ·cm and transmittance over 85% are obtained for thin films sputtered under optimum conditions. Iron doping results in significant improvement in films transmittance and increasing the crystallization temperature of ITO thin films.

Key words: iron-doped indium-tin oxide, electrical properties, optical properties, magnetron direct current sputtering, radio frequency deposition.

Corresponding author: Svitlana Stepanivna Petrovska
E-mail: sw.piotrowska@gmail.com

Citation: M. Ohtsuka, R. Sergiienko, S. Petrovska, B. Ilkiv, and T. Nakamura, Effect of Sputtering Power on Optoelectronic Properties of Iron-Doped Indium Saving Indium-Tin Oxide Thin Films, *Metallofiz. Noveishie Tekhnol.*, **41**, No. 7: 941–952 (2019), DOI: 10.15407/mfint.41.07.0941.

Тонкі плівки оксиду індію-олова (ОІО), леговані залізом зі зниженим до 50% мас. вмістом оксиду індію, осаджувалися на скляні підкладки, попередньо нагріті при 523 К, шляхом одночасного напорошення мішеней ОІО і Fe_2O_3 у змішаній атмосфері аргон-кисень. Вплив різних потужностей високочастотного напорошення мішені Fe_2O_3 на електричні, оптичні, структурні і морфологічні властивості плівок досліджено за допомогою чотирьохточкового методу, ультрафіолетової–видимої–інфрачервоної (УФ–Вид–ІЧ) спектроскопії, рентґенівської дифракції і атомної силової спектроскопії. Об'ємний опір порядку 930 мкОм·см і пропускання вище 85% отримано для плівок, осаджених за оптимальних умов. Легування залізом призводить до помітного збільшення пропускання світла видимої частини спектра і підвищує температуру кристалізації тонких плівок ОІО.

Ключові слова: легований залізом оксид індію-олова, електричні властивості, оптичні властивості, магнетронне розпилення на постійному струмі, високочастотне напорошення.

Тонкие плёнки оксида индия-олова (ОИО), легированные железом со сниженным до 50% масс. содержанием оксида индия, осаждались на стеклянные подложки, предварительно нагретые при 523 К, путём совместного напыления мишеней ОИО и Fe_2O_3 в смешанной атмосфере аргон-кислород. Влияние разных мощностей высокочастотного напыления Fe_2O_3 мишени на электрические, оптические, структурные и морфологические свойства плёнок было исследовано с помощью четырёхточечного метода, ультрафиолетовой–видимой–инфракрасной (УФ–Вид–ИК) спектроскопии, рентгеновской дифракции и атомной силовой спектроскопии. Объёмное сопротивление порядка 930 мкОм·см и пропускание выше 85% получены для плёнок, осаждённых при оптимальных условиях. Легирование железом приводит к заметному увеличению пропускания света видимой части спектра и повышает температуру кристаллизации тонких плёнок ОИО.

Ключевые слова: легированный железом оксид индия-олова, электрические свойства, оптические свойства, магнетронное распыление на постоянном токе, высокочастотное напыление.

(Received October 22, 2018; in final version—February 12, 2019)

1. INTRODUCTION

Indium tin oxide thin films have potential application as transparent conducting materials for solar cells, optical solar reflectors and panel displays [1–3], because of their well-known physical properties such as low resistivity and high transmittance in the visible wavelength region. The most preferred method of ITO thin films production is sputtering using ITO targets [4, 5] due to its good reproducibility and adhesion of the films to the substrates and high deposition rate. ITO targets with 5–10% mass SnO_2 have been usually used for the ITO sputtered thin films with good optoelectronic properties [6]. However natural supply of indium is limited. Therefore in order to decrease the use

of indium during the production of ITO films, a new target with smaller quantity of In_2O_3 in its composition is required to be developed.

Studies of undoped ITO sputtered thin films with reduced amount of In_2O_3 were reported in [7–11]. Minami *et al.* [7–9] reported In_2O_3–SnO_2 films with 50% mol of Sn deposited by DC magnetron sputtering; it had high transmittance and conductivity. Minami *et al.* [7] found that resistivity and transmittance of ITO thin films were strongly dependent on the O_2 gas content. Promising optoelectronic properties were obtained in [10] for ITO50 thin films deposited by DC sputtering onto preheated to 523 K substrates. RF magnetron sputtering was applied for deposition of highly conductive and transparent In_2O_3–SnO_2 films with 50% mass of SnO_2 in [11]. Influence of oxygen flow rate on properties of ITO thin films was studied by Li *et al.* [11].

Recently, our research group has investigated the structural, electrical and optical properties of the indium saving ITO thin films of In_2O_3-50% mass SnO_2 (ITO50) doped with titanium oxide [12] as an alternative to conventional ITO. It allowed achieving low resistivity of 31.7 μΩ·m and high transmittance in visible range (over 85%). Dependence of optoelectronic properties of iron-doped ITO50 thin films on oxygen flow rate and heat treatment temperature was revealed in [13].

In this study, iron-doped ITO50 thin films were produced by co-sputtering method onto glass substrates preheated at 523 K (ITO50: Fe_2O_3 (PHS)). In order to reduce indium usage in ITO films, an amount of indium oxide in the target was decreased from 90% mass to 50% mass. Effect of heat treatment temperature and RF power applied for sputtering of Fe_2O_3 target on structural and optoelectronic properties of ITO50: Fe_2O_3 (PHS) thin films were studied.

2. EXPERIMENT

Iron-doped ITO50 (ITO50: Fe_2O_3) thin films were co-sputtered from ceramic ITO50 (Mitsui Mining & Smelting, In_2O_3 and 48.9% mass SnO_2) and Fe_2O_3 (Kojundo Chemical Laboratory, 99.9% mass) targets on glass substrates (Corning EAGLE 2000, surface: 50 mm × 50 mm, thickness: 0.7 mm) preheated at 523 K (PHS) by using a commercial sputtering system ULVAC, CS-200 (Fig. 1). Process chamber was evacuated down to a base pressure of 10^{-5} Pa while total experimental pressures were between 0.67 and 0.69 Pa. The DC plasma power W_{DC} for sputtering of ITO50 target was kept at 100 W. The RF plasma power for sputtering of Fe_2O_3 target $W_{RF}(Fe_2O_3)$ was altered from 0 to 100 W. The composition of the film was determined by inductively coupled plasma (ICP) method, the iron content depends on the RF power source and iron oxide content reached about 0.1% mass at power of 20 W and about 1.7% mass at power of 100 W (Table 1).

The argon gas flow rate was kept constant at $Q(\mathrm{Ar}) = 50$ sccm and

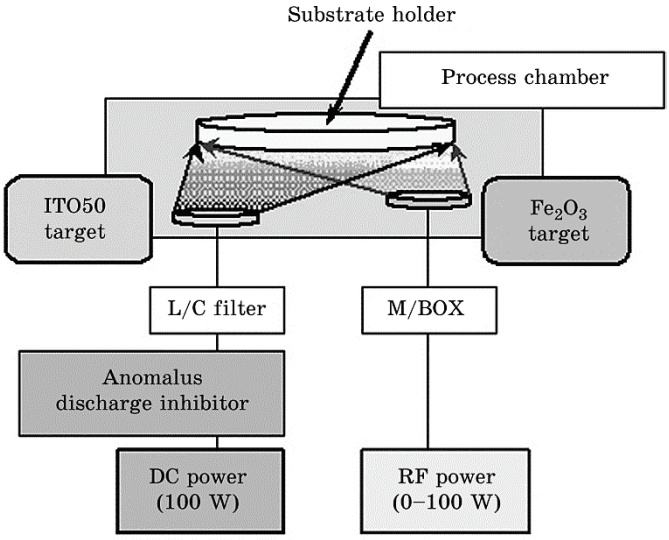

Fig. 1. Schematic diagram of the sputtering apparatus.

oxygen gas flow rate $Q(O_2)$ was fixed at 0.2 sccm. The deposition time was set at 30 min. The deposited films were heat-treated in air at 523–923 K (HT523–HT923) for 60 min and cooled to room temperature in the furnace.

In order to determine the thickness for the obtained films, a very thin line of about 50 μm of width and 1 mm of length was removed with a laser (LaserX, LXSY-UV) in several aligned positions separated 10 μm to each other and then thickness was measured in each of those positions by using a scanning probe microscope (SPM, SII L-trace II), under dynamic force mode (DFM).

The volume resistivity ρ_v of the films was measured with a resistivity

TABLE 1. Elements' and oxide compositions of ITO50: Fe_2O_3 (PHS) thin film sputtered at $Q(Ar)/Q(O_2) = 50$ sccm/0.2 sccm.

Elements	% mass	Oxides	% mass
Data from ICP, $W_{RF}(Fe_2O_3) = 20$ W			
In	52.60	In_2O_3	51.40
Sn	47.31	SnO_2	48.50
Fe	0.09	Fe_2O_3	0.10
Data from ICP, $W_{RF}(Fe_2O_3) = 100$ W			
In	49.60	In_2O_3	48.30
Sn	48.90	SnO_2	50.00
Fe	1.50	Fe_2O_3	1.70

meter (Mitsubishi chemical analytech, Loresta GP Model MCP-T610) by a 4-terminal method using the obtained thickness information in accordance with Japanese Industrial Standards JIS K 7194-1994.

Optical transmittance τ of the films was recorded into the (200–2600 nm) nm range of wavelength with a spectrophotometer (Hitachi High-Tech, U-4100).

The structural properties of the films for different heat-treated temperatures (523–923 K) were determined by X-ray diffraction using a Rigaku Rint-2000 diffractometer with CuK_α (0.15418 nm) radiation.

Surface properties were investigated for the as-deposited (as-depo.) ITO50: Fe_2O_3 thin films in comparison to undoped ITO50 (PHS) and typical ITO90 (PHS) (In_2O_3–10% mass SnO_2) by using a SPM under the DFM.

3. RESULTS AND DISCUSSION

3.1. Deposition Rate

Figure 2 shows the relation between the deposition rate d of the ITO50: Fe_2O_3 thin films and the RF power of Fe_2O_3 target $W_{RF}(Fe_2O_3)$. The d value was increased from 4.53 to 4.97 nm/min with increasing $W_{RF}(Fe_2O_3)$ from 0 to 40 W since more species of Fe_2O_3 target were sputtered and deposited onto glass substrates with increasing $W_{RF}(Fe_2O_3)$.

3.2. Optoelectronic Properties

It can be seen that the volume resistivity ρ_v of the ITO50: Fe_2O_3 (PHS) thin films is affected greatly by the RF power of the Fe_2O_3 target $W_{RF}(Fe_2O_3)$ (Fig. 3). The ρ_v of the as-deposited films has minimum at 10 W (930 $\mu\Omega$·cm) and increases with increasing $W_{RF}(Fe_2O_3)$ above

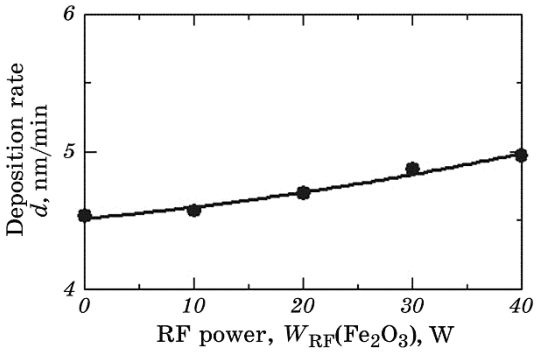

Fig. 2. Deposition rate of ITO50: Fe_2O_3 (PHS) thin films at different RF powers.

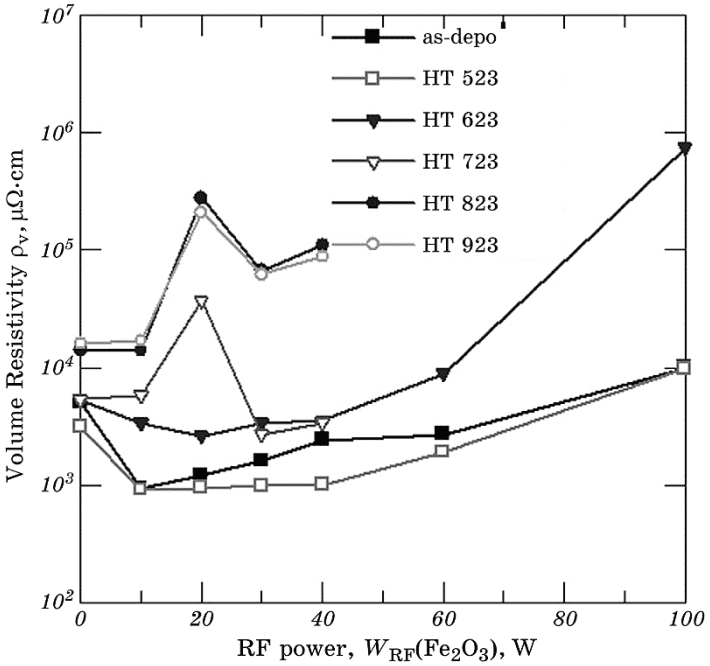

Fig. 3. Effect of RF power of Fe_2O_3 target and heat treatment temperature on volume resistivity of the ITO50: Fe_2O_3 (PHS) thin films.

10 W. This may be connected with dying out of doping effect of iron oxide that does not create additional charge carrier anymore and behaves like neutral scattering centre.

The decrease of volume resistivity of ITO50: Fe_2O_3 (PHS) films heat-treated at 523 K (HT523) with increasing $W_{RF}(Fe_2O_3)$ to 10 W was due to increases in mobility and carrier density in the films (Fig. 4). As can be seen from Fig. 4, the mobility of as-deposited and HT523 ITO50: Fe_2O_3 (PHS) films increases with increasing $W_{RF}(Fe_2O_3)$ showing maximum at 30 W and then decreases. The carrier density of as-deposited thin films decreases with increasing $W_{RF}(Fe_2O_3)$ (Fig. 4). The carrier density of HT523 thin films increases with increasing $W_{RF}(Fe_2O_3)$ to 10 W and then decreases.

Minimal values of volume resistivity for HT523 thin films were obtained in a wide range of $W_{RF}(Fe_2O_3)$ from 10 to 40 W. Further increases in the heat treatment temperature cause a sharp increase in the resistivity due to chemisorption of oxygen on the film surface at high temperature when heat treating in air [14].

The transmittance (τ) of the as-deposited ITO50: Fe_2O_3 (PHS) thin films at a light wavelength of 550 nm abruptly increases with increasing $W_{RF}(Fe_2O_3)$ to 10 W (Fig. 5), keeping high value with some devia-

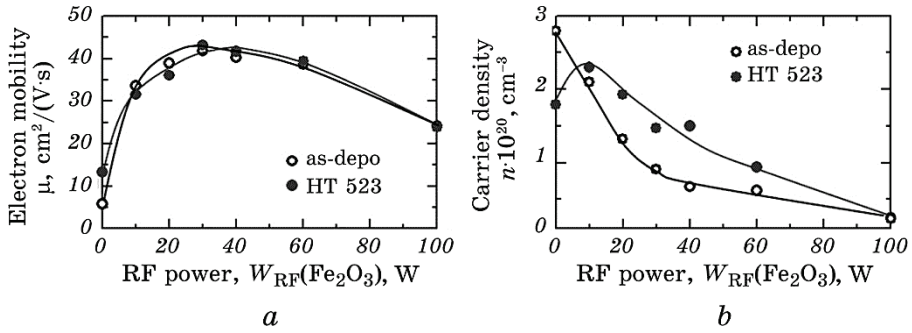

Fig. 4. The electron mobility (*a*) and the carrier density (*b*) of the as-deposited and HT523 ITO50: Fe_2O_3 (PHS) thin films deposited at optimum flow rate of $Q(Ar)/Q(O_2) = 50$ sccm/0.2 sccm depending on $W_{RF}(Fe_2O_3)$.

tions up to 100 W, making these films particularly attractive from an optical point of view.

The values of τ at wavelength range of 200–800 nm for the ITO50: Fe_2O_3 (PHS) thin films deposited at different $W_{RF}(Fe_2O_3)$ (10–100 W) are very close to each other. While in infrared (IR) region (800–

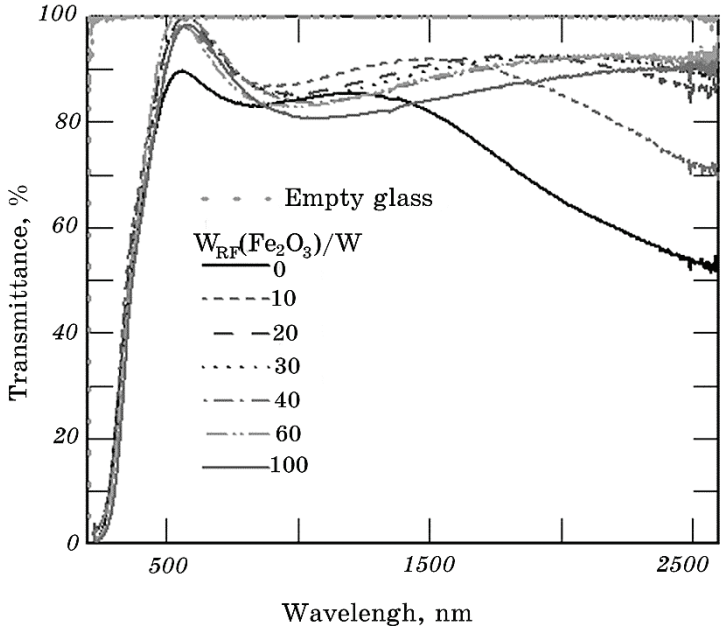

Fig. 5. Effect of RF power on transmittance of the as-deposited ITO50: Fe_2O_3 (PHS) films. The transmittance was measured by using substrate glass as reference sample.

2200 nm) the difference in optical properties increased for different $W_{RF}(Fe_2O_3)$.

The deviations between the optical properties of deposited films are minimal at values of RF power equal to 20–60 W at whole wavelength range. Increasing transmittance of as-deposited ITO50: Fe_2O_3 (PHS) films in visible region is associated with the fact that iron oxide is an additional source of oxygen during filling of oxygen vacancies.

3.3. Structural Properties

Figure 6 shows the XRD pattern of ITO thin films deposited at $W_{RF}(Fe_2O_3) = 10$ W heat treated at various temperatures. The as-deposited film did not show any X-ray diffraction peaks so this film may be regarded as amorphous. The hump between $2\theta = 20°$ and 30° is

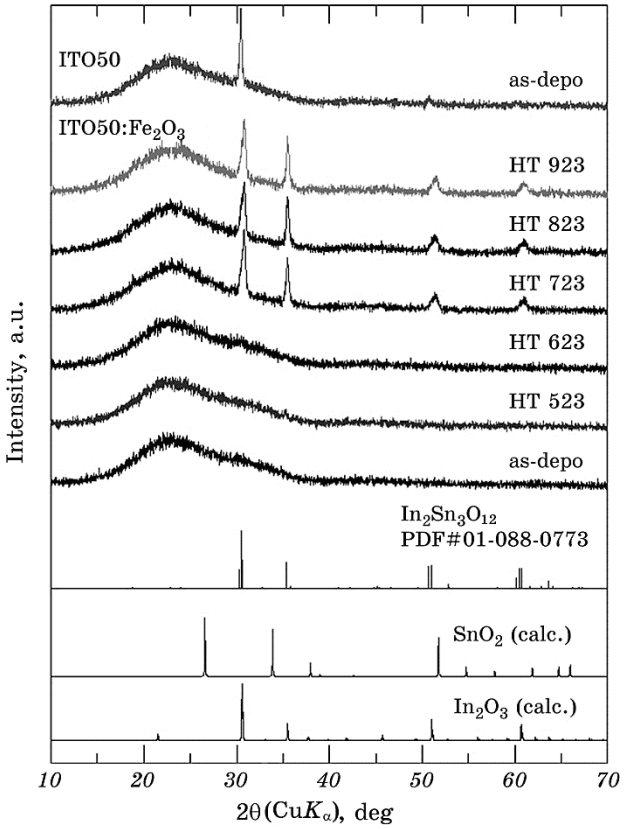

Fig. 6. XRD results for the as-deposited and HT523-923 ITO50: Fe_2O_3 (PHS) films deposited under $W_{RF}(Fe_2O_3) = 10$ W, $Q(Ar)/Q(O_2) = 50$ sccm/0.2 sccm [13] and as-deposited ITO50 (PHS) [13].

owing to the background of the glass substrates. The XRD pattern for the same sample, recorded after its heat-treatment at 723 K is polycrystalline with peaks corresponding to $In_4Sn_3O_{12}$ [15, 16]. Iron oxide phases are absent on the observed XRD patterns. Doping by Fe_2O_3 does not change the structure of ITO50 thin films since possibly iron embedded in ITO thin films and formed ordered substitutional sites within the lattice as it was observed for iron-doped ZnO thin films [17, 18] or iron oxide content is too small to be detected by XRD.

Increasing of RF power to 10 W hindered the crystallization of the ITO50: Fe_2O_3 (PHS) thin films deposited at $W_{RF}(Fe_2O_3) = 10$ W and $Q(Ar)/Q(O_2) = 50$ sccm/0.2 sccm since iron-doped ITO50 thin films crystallizes at higher temperature than undoped ITO50 ($Q(Ar)/Q(O_2) =$ = 50 sccm/0.2 sccm) which crystallizes in as-depo state.

Figure 7 shows surface analysis results for the as-depo ITO50:Fe_2O_3 (PHS) films deposited under different powers $W_{RF}(Fe_2O_3) = 10–40$ W and at $Q(Ar)/Q(O_2) = 50$ sccm/0.2 sccm. It is clear that film deposited at $W_{RF}(Fe_2O_3) = 10$ W shows smooth and uniform surface, while with increasing $W_{RF}(Fe_2O_3)$ some imperfections appear. As can be seen from Table 2, root mean square height (S_q) and arithmetical mean height (S_a) increase with increasing of $W_{RF}(Fe_2O_3)$.

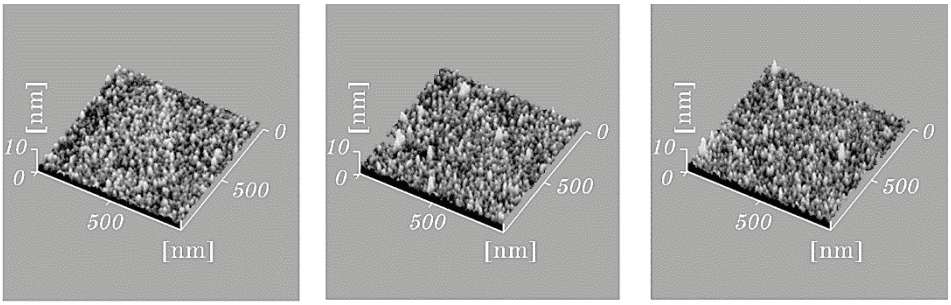

a *b* *c*

Fig. 7. Surface analysis results for the as-deposited ITO50: Fe_2O_3 (PHS) thin films deposited at $Q(Ar)/Q(O_2) = 50$ sccm/0.2 sccm and different RF powers of $W_{RF}(Fe_2O_3)$: *a*—10 W, *b*—20 W, *c*—40 W.

TABLE 2. Root mean square height (S_q) and arithmetical mean height (S_a) of as-depo ITO50: Fe_2O_3(PHS) thin films.

RF power, $W_{RF}(Fe_2O_3)$, W	Root mean square height, S_q, nm	Arithmetical mean height, S_a, nm
10	0.71	0.56
20	0.83	0.63
40	0.91	0.68

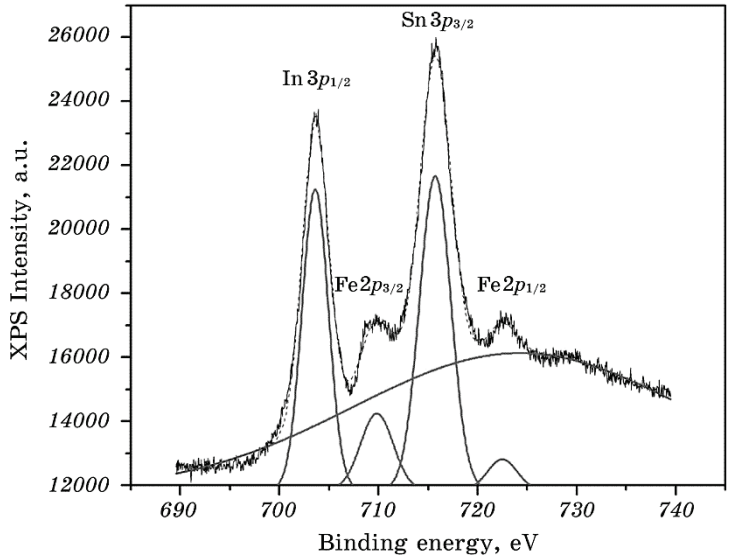

Fig. 8. Curve fitting by Gaussian of the XPS core level spectrum Fe 2*p* of the PHS523 ITO50: Fe_2O_3 film deposited at RF 100 W (after Ar sputtering at 3 kV for 1 min).

TABLE 3. Results of curve fitting for Fe 2*p* peaks of PHS523 ITO50: Fe_2O_3 thin film after Ar sputtering at 3 kV for 1 min by Gaussian lines.

Peaks	Position, eV
In $3p_{1/2}$	703.62
Fe $2p_{3/2}$	709.84
Sn $3p_{3/2}$	715.72
Fe $2p_{1/2}$	722.49

3.4. XPS ANALYSIS

Figure 8 shows the XPS core levels of Fe 2*p* of the ITO50: Fe_2O_3 (PHS) thin films. After Ar sputtering at 3 kV for 1 min Fe 2*p* peaks were deconvoluted. The binding energy of Fe $2p_{3/2}$ is 709.84 eV (Table 3) showing the Fe^{2+} bonding state from FeO [19].

4. CONCLUSION

Iron-doped indium tin oxide (ITO) thin films with reduced 50% mass indium oxide content were deposited onto glass substrates preheated at 523 K (PHS) by co-sputtering method at different radio frequency

powers of Fe_2O_3 target and subsequently heat treated.

1. Increasing a high radio frequency power from 0 to 10 W significantly improves the transmittance of ITO50: Fe_2O_3 (PHS) thin films at fixed oxygen flow rate $Q(O_2) = 0.2$ sccm since iron oxide is an additional source of oxygen during filling of oxygen vacancies. Even at $W_{RF}(Fe_2O_3) = 10$ W, transmittance at 550 nm is 97.9%, but the films deposited at $W_{RF}(Fe_2O_3) = 20–60$ W have minimal differences between the optical properties at whole wavelength range.
2. The best obtained values of volume resistivity (930 μΩ·cm) for the ITO50: Fe_2O_3 (PHS) thin films was derived at $W_{RF}(Fe_2O_3) = 10$ W without any heat treatment. Further increase of $W_{RF}(Fe_2O_3)$ power conduces to increase of volume resistivity. This may be connected with dying out of doping effect of iron oxide.
3. Increasing high radio frequency power from 0 to 10 W hindered the crystallization of the thin film.
4. Increasing $W_{RF}(Fe_2O_3)$ power causes increasing the ITO50: Fe_2O_3 films (PHS) roughness.

The present research was supported by New Energy and Industrial Technology Development Organization (NEDO), Japan.

REFERENCES

1. K. P. Sibin, G. Srinivas, H. D. Shashikala, A. Dey, N. Sridhara, A. K. Sharma, and H. C. Barshilia, *Sol. Energy Mater. Sol. Cells,* **145**, Iss. 4, Part 3: 10787 (2018).
2. Z. Meng, H. Peng, C. Wu, C. Qiu, K. K. Li, M. Wong, and H. S. Kwok, *J. Soc. Inform. Display*, **12**: 113 (2004).
3. C. Hengst, S. B. Menzel, G. K. Rane, V. Smirnov, K. Wilken, B. Leszczynska, D. Fischer, and N. Prager, *Materials*, **10**: 245 (2017).
4. O. Tuna, Y. Selamet, G. Aygun, and L. Ozyuzer, *J. Phys. D: Appl. Phys.*, **43**, No. 5: 055402-1 (2010).
5. Z. Ghorannevis, E. Akbarnejad, and M. Ghoranneviss, *J. Theor. Appl. Phys.*, **9**, Iss. 4: 285 (2015).
6. Sh.-Ch. Her and Ch.-F. Chang, *J. Appl. Biomater. Funct. Mater.*, **15**, Iss. 2: 170 (2017).
7. T. Minami, Y. Takeda, S. Takata, and T. Kakumu, *Thin Solid Films*, **308–309**: 13 (1997).
8. T. Minami, T. Miyata, and T. Yamamoto, *Surf. Coat. Tech.*, **108–109**: 583 (1998).
9. T. Minami, T. Kakumu, K. Shimokawa, and S. Takata, *Thin Solid Films*, **317**, Iss. 1–2: 318 (1998).
10. L. Voisin, M. Ohtsuka, S. Petrovska, R. Sergiienko, and T. Nakamura, *Optik*, **156**: 728 (2018).
11. S. Li, X. Qiao, and J. Chen, *Mater. Chem. Phys.*, **98**: 144 (2006).
12. L. Voisin, M. Ohtsuka, and T. Nakamura, *Mater. Trans.*, **51**, Iss. 3: 503 (2010).
13. M. Ohtsuka, R. Sergiienko, S. Petrovska, B. Ilkiv, and T. Nakamura, *Optik*, **179**: 19 (2019).

14. H. A. Mohamed, *J. Phys. D Appl. Phys.*, **40**, No. 14: 4234 (2007).
15. W. J. Heward and D. J. Swenson, *J. Mater. Sci.*, **42**, Iss. 17: 7135 (2007).
16. N. Nadaud, M. Nanot, J. Jové, and T. Roisnel, *Key Eng. Mater.*, **132–136**: 1373 (1997).
17. L. Xu and X. Li, *J. Cryst. Growth*, **312**, Iss. 6: 851 (2010).
18. F. Gao, X. Y. Liu, L. Y. Zheng, M. X. Li, Y. M. Bai, and J. Xie, *J. Cryst. Growth*, **371**: 126 (2013).
19. J. F. Moulder, W. E. Stickle, P. E. Sobol, and K. E. Bomben, *Handbook of X-Ray Photoelectron Spectroscopy* (Minnesota, Perkin-Elmer Corporation: 1992).